Empirical Validation of Soil Temperature Sensing Depth Derived From the Tau-z Model Utilizing Data From the Soil Moisture Experiment in the Luan River (SMELR)

Shaoning Lv, Tianjie Zhao, *Senior Member, IEEE*, Yin Hu, and Jun Wen

***Abstract*—Soil moisture is a critical variable in climate forecasting, hydrology, and others. Satellite-based remote sensing techniques have been used to map soil moisture globally, including visual bands, infrared, Synthetic Aperture Radar (SAR), passive microwave remote sensing, etc. Passive microwave remote sensing techniques, especially at the *L*-band, such as the Soil Moisture and Ocean Salinity (SMOS) and Soil Moisture Active Passive (SMAP), have higher accuracy than the others due to their higher sensitivity to the dielectric constant of the soil profile. However, the unclear sensing depth at *L*-band for SMOS and SMAP leads to a mismatch in the calibration/validation and application of their soil moisture products. In this study, we apply soil temperature sensing depth model, i.e., the tau-z model, to the soil temperature, soil moisture, and brightness temperature (TB) data collected during the Soil Moisture Experiment in the Luan River (SMELR). The effectiveness of the tau-z model in interpreting the *L*-band microwave observations is validated through forward simulations with the Community Microwave Emission Modelling (CMEM). Results showed that: 1) the bias in TB simulation can be reduced from 26.22 K/12.00 K to -11.66 K/-8.839 K for H/V-polarization; 2) the RMSE is reduced from 30.2 K/20.48 K to 12.92 K/11.66 K for H/V-polarization by considering the microwave sensing depth. Daily TB signal variation partly attributed to the soil temperature sensing depth due to different bands' penetration capacity. The result is expected to improve the understanding of microwave data collected by muli-frequency synthetic platforms such as Copernicus Microwave Imaging Radiometer (CIMR).**

***Index Terms*—Passive microwave, penetration depth, soil moisture, soil optical depth, soil temperature sensing depth.**

Manuscript received 2 April 2024; revised 13 June 2024; accepted 30 June 2024. Date of publication 13 August 2024; date of current version 5 September 2024. This work was supported in part by the National Natural Science Foundation of China under Grant 42075150, in part by the National Key Research and Development Program of China under Grant 2022YFF0801404, in part by the Natural Science Foundation of Shanghai under Grant 21ZR1405500, in part by the National Key Research and Development Program of China under Grant 2021YFB3900104, and in part by Nordic Centre Planning Grant Seed funding for Sino-Nordic research collaboration: Microwave remote sensing monitoring of summertime sea ice change and the impact from high-latitude synoptic weather systems. *(Corresponding author: Tianjie Zhao.)*

Shaoning Lv is with the Department of Atmospheric and Oceanic Sciences (Institute of Atmospheric Sciences), Fudan University, Shanghai 200438, China, also with the Zhuhai Fudan Innovation Research Institute, Zhuhai 519000, China, also with the Shanghai Key Laboratory of Ocean-Land-Atmosphere Boundary Dynamics and Climate Change, Fudan University, Shanghai 200438, China, and also with the Key Laboratory of Polar Atmosphere-Ocean-Ice System for Weather and Climate, Ministry of Education, Fudan University, Shanghai 200438, China (e-mail: lvshaoning@fudan.edu.cn).

Tianjie Zhao is with the State Key Laboratory of Remote Sensing Science, Aerospace Information Research Institute, Chinese Academy of Sciences, Beijing 100101, China (e-mail: zhaotj@aircas.ac.cn).

Yin Hu is with the Department of Atmospheric and Oceanic Sciences (Institute of Atmospheric Sciences), Fudan University, Shanghai 200438, China (e-mail: 22213020008@m.fudan.edu.cn).

Jun Wen is with the The Plateau Atmosphere and Environment Key Laboratory of Sichuan Province, Chengdu University of Information Technology, Chengdu 610225, China (e-mail: jwen@cuit.edu.cn).

Digital Object Identifier 10.1109/JSTARS.2024.3434414

I. Introduction

SOIL moisture demonstrates a distinct hysteresis response to alterations in surface fluxes induced by precipitation, commonly called the "memory effect." This hysteresis significantly amplifies and extends the feedback mechanisms contributing to climate anomalies, manifesting itself over several weeks to entire seasons [1], [2]. Additionally, spatial variation in soil moisture also strongly affects the occurrence and development of mesoscale convective weather systems [3], [4]. However, current land surface and hydrological models are still insufficient to accurately simulate soil moisture's spatial and temporal changes [5]. Still, the research results of the African monsoon multidisciplinary analysis land surface model (LSM) intercomparison project show that none of the existing LSMs can simulate soil moisture well, among which soil hydrological parameters and forcing assimilation of various observational data based on the LSMs are currently considered to be a feasible and relatively effective way to establish a global soil moisture dataset [6], [7]. More accurate soil moisture temporal–spatial distribution data products on a global scale are needed [8], and remote sensing techniques are developed to provide either soil moisture retrievals or observation input for data assimilation.

After 50 years of development, passive microwave remote sensing has become a significant method for obtaining soil moisture [9]. In 1973, data from the SkyLab space station began being studied using passive microwave remote sensing to conduct soil moisture research [10], [11]. In the early 1970s, the National Aeronautics and Space Administration conducted a flight test of an airborne microwave radiometer in the Alexandria farmland [12]. It simultaneously observed the soil moisture at 0–15 cm depths and found a strong correlation between the brightness temperature (TB) and soil moisture. After 1978, satellite microwave remote sensing data, such as the scanning multichannel microwave radiometer and the special sensor microwave/imager on the Nimbus satellite and DMSP (the National Defense Meteorological Satellite), began to be effectively used [13]. However,

TABLE I
DEPTH DEFINITIONS REFERRED TO IN THIS STUDY

Depth name	symbol	definition	remark
Penetration depth	/	the depth in 1/e attenuation from the surface	$\tau=1$
Sensing depth	/	Including Soil temperature sensing depth and Soil moisture sensing depth	No rigorous mathematical definition is available
Soil temperature sensing depth	z_{Teff}	the mean emission value for a profile regarding soil temperature	This can be inferred from the Tau-Z model.
Soil moisture sensing depth	/	the mean emission value for a profile regarding soil moisture	No rigorous mathematical definition is available

they are greatly affected by vegetation and the atmosphere, and further to soil moisture retrieval. The advanced microwave scanning radiometer for the Earth observing system inherits the advantageous bands of previous microwave radiometers and adds additional bands, which can provide dual polarization and multifrequency brightness temperature data in the frequency range from 6.9 to 89 GHz [14]. Soil moisture inversion can be performed in the *C*-band [15], where the 6.9 GHz frequency channel is located. In 2009, the European Space Agency's (ESA) second Earth observation program, soil moisture and ocean salinity (SMOS), was successfully launched [16]. Its payload, microwave imaging radiometer with aperture synthesis, is an *L*-band, 2-D, dual-polarization, and passive microwave interference radiometer, which cannot only measure sea surface salinity but also monitor global soil moisture [17]. Soil moisture active passive (SMAP) [18] has provided a global soil moisture map since 2015 [19]. Currently, passive microwave remote sensing technology can obtain high-resolution and high-precision surface soil moisture data, providing critical support for research and applications [20], [21], [22].

In general, passive microwave remote sensing can only obtain the soil moisture at the top layer, and the remote sensing capabilities for deeper soil moisture and even soil moisture profiles are relatively lacking. Soil moisture sensing depth (see Table I) is necessary to discuss the true sensing capabilities of each band. While penetration depth is defined as the depth in 1/e attenuation from the surface, soil temperature sensing depth is considered the mean emission value for a profile [23], [24], which sources from the definition of soil effective temperature [25], [26], [27]. Compared with visible light, infrared, ultraviolet, and other bands that realized spaceborne observation earlier, the microwave, especially for the low bands from 1 to 100 GHz, is yet to be completed [28], [29], [30]. Because the *L*-band (1–2 GHz) and *P*-band (0.75 GHz) are sensitive to soil moisture and less affected by weather, vegetation, and human interference sources, its related land surface products have been widely used. It has dramatically improved the radiative transfer theory role [31], [32], [33], [34], [35]. These bands have greater penetration capability into the soil; theoretically, they could reach up to 40 cm for the *P*-band and 10 cm for the *L*-band.

However, the issue with unclear soil moisture sensing depth has obscured the passive microwave remote sensing of soil moisture until now. Without knowing the sensing depth, it would be the following.

1) The calibration/validation of SMAP and SMOS soil moisture products lacks enough evidence to configure the installation depth of sensors and increases errors in the result.
2) The lapse rate and evaporation rate of soil moisture are underestimated, which leads to wrong flux in land–atmosphere interaction.
3) Making it more complicated in comparing soil moisture products among different bands, such as *C/L/P*-bands, where layer precisely corresponds to the soil moisture retrieval from the *L/P*-band is not fixed yet [31], [36], [37].

In this study, the tau-z model [24], which is math derived and has a fixed solution, is applied to TB and soil temperature (T)/moisture (θ) profile in the soil moisture experiment in the Luan River (SMELR) to evaluate its effectiveness in improving the dynamic of the sensing depth [38].

The rest of this article is organized as follows. Section I introduces the background of this research. Section II proposes the experiment and the data used here. Section III describes the community microwave emission modeling platform (CMEM) [30], [39], which is used for forwarding simulation, and the tau-z model. We analyze the results by considering the fixed 5-cm/penetration depth/soil temperature sensing depth (z_{Teff}) in Section IV. Discussion is posted in Section V. Finally, Section VI concludes this article.

II. EXPERIMENT AND DATA

The SMELR, which was conducted in the summer of 2018, provides all the input data used in this study. The test site is in Xinyuan Ranch (115.93°E, 42.04°N) in Zhenglanqi, China (see Fig. 1, [38]). The dataset contains the multifrequency and multiangle ground-based microwave radiometer and radar active/passive microwave backscatter/TB data, T/θ profile, and measurements of vegetation and soil parameters related to microwave remote sensing. The RPG-6CH-DP vehicle-mounted microwave radiometer obtains the microwave TB data, including the *L*-band horizontal- and vertical-polarization TB. The data measurement interval is 0.5 h. The observed incident angle varies from 30° to 65° (2.5° interval), and the azimuth angle varies at 340°, 340°, 0°, and 20°. Since this study focuses on the *L*-band passive microwave remote sensing data, we take only TB data at 40° in coincidence with SMAPs configuration.

The soil data include surface roughness parameters (see Table II), rainfall data from the HOBO rain gauge [see Fig. 2(a)], T, and θ of six layers at 1, 3, 5, 10, 20, and 50 cm [see Fig. 2(b) and (c)]. The profile measurement is conducted using the Decagon 5TM sensor, with a precisely oriented and tilted 1-cm layout to ensure accuracy and reliability. The sampling interval

Fig. 1. Landscape of the comprehensive remote sensing experiment of the water cycle and energy balance in the SMELR.

TABLE II
SURFACE ROUGHNESS PARAMETERS

Month	August			September			
Day	17	24	31	7	14	21	26
The mean value of root-mean-square height (cm)	1.03	1.21	1.44	1.33	1.3	1.34	1.13
The mean value of correlation length (cm)	24.1	13.6	13.8	19.5	18	22.2	17.3

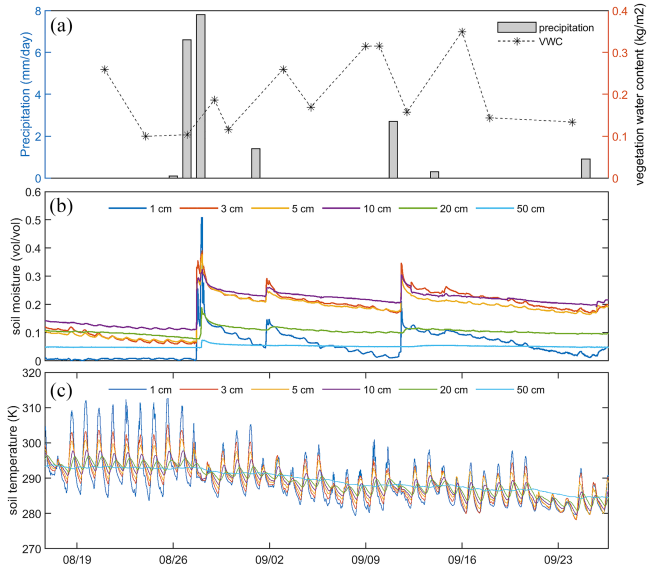

Fig. 2. Input data for driving CMEM from 18 August to 25 September 2018. (a) Rainfall and vegetation water content. (b) Soil moisture (θ). (c) Soil temperature (T) time series observed at a depth of 1 cm/3 cm/5 cm/10 cm/20 cm/50 cm.

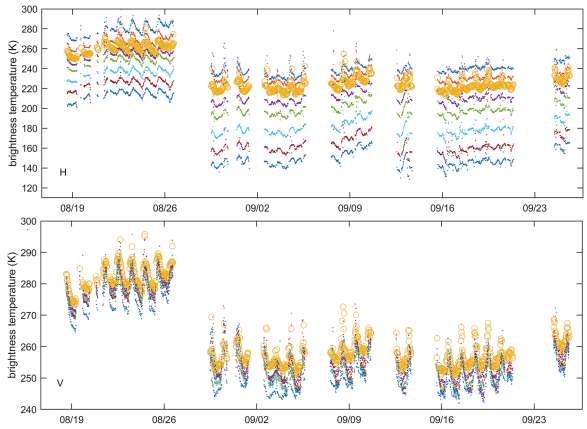

Fig. 3. Incidence angles of TB at 30°–65° from 16 August to 26 September 2018. (a) H-polarization and (b) V-polarization at the L-band.

is 10 min, and we only adapt the moment coincidence with the radiometer measurement at each half an hour. The vegetation data are grassland vegetation moisture content [see Fig. 2(a)]. Both surface roughness and vegetation are interpolated to 30-min intervals with the linear method.

The experimental observation lasted from 18 August to 25 September 2018. Five rainfall events happened on 28 and 29 August, and 1, 11, 14, and 25 September [see Fig. 2(a)]. θ immediately responds to these rainfall events [see Fig. 2(b)]. Before 28 August, θ at all layers was very dry ($\theta \leq 0.15$ cm^3/cm^3), among which 1 cm shows parched soil, almost without measurable soil moisture values. Still, in this period, T has a higher daily variation ($\Delta T \leq 25$ K at 1 cm) than the rest time ($\Delta T \leq 15$ K at 1 cm). TB from 16 to 28 August indicates higher H/V-polarization values of 50 K/30 K compared with the rest time (see Fig. 3). On 28 August, the 1-cm soil moisture showed the maximum value in this experiment, nearly 0.5 cm^3/cm^3, but it was draining faster than all other layers. For instance, the soil moisture at 1 cm decreased from 0.5 to 0.08 cm^3/cm^3 in four days, which is 0.1 cm^3/cm^3 per day. This phenomenon can be attributed to the exposure of shallow soil layers to solar radiation and dry atmospheric conditions, resulting in enhanced evaporation rates during sunny days. Compared with 1 cm, θ at 3 cm/5 cm/10 cm shows a relatively consistent draining speed, i.e., 0.03 cm^3/cm^3 per day, and the daily variation of soil temperature is also more minor than the days before 28 August due to increased soil heat capacity. Additionally, at 50 cm depth, T and θ variations are insignificant likely due to reduced surface influence. Instead, they are more influenced by groundwater and deeper soil layers.

III. METHODOLOGY

A. CMEM Model

This study simulates TB at the L-band with the CMEM model, which was developed by the European Centre for Medium-Range Weather Forecasts (ECMWF) and serves as the forward operator for low-frequency passive microwave brightness temperatures ranging from 1 to 100 GHz at the surface [28], [40]. CMEM is a new, highly modular code providing I/O interfaces for the numerical weather prediction (NWP) community and

is based on a simplified 1-D solution of the radiative transfer equation for a multilevel medium. So, CMEM modularity allows for considering different parametrizations of the soil dielectric constant and various modules (coherent or incoherent), as well as effective temperature, roughness, snow, vegetation, and atmospheric contribution opacity schemes. SMOS brightness temperatures are used at ECMWF to investigate its use in analyzing soil moisture through the surface data assimilation system and monitoring ocean salinity. This is expected to improve the accuracy of the initial conditions of the NWP model. NWP products are essential for space agencies to derive the Level 2 SMOS products.

In detail, CMEM contains various modules for land types, such as low/high vegetation cover and open snow-covered water. Since the experiment only has grassland in summer, we simplified the CMEM model with only its smooth soil emissivity, roughness, and vegetation modules. A new soil effective temperature (T_{eff}) module named Lv model [41], [42] replaces CMEMs T_{eff} to include soil optical depth (for details, see Section III-B). The atmosphere's attenuation could be safely ignored except for intense precipitation, which did not occur in the experiment during the period discussed. According to Planck and Kirchhoff's laws, each soil layer emits radiation in the Fresnel scheme, attenuated in adjacent layers through absorption and scattering processes, determined by their optical depths and scattering properties. For polarization p, TB at the top of the atmosphere ($T_{B\text{toa}.p}$), for example, as measured by a satellite and at the top of the vegetation ($T_{B\text{tov}.p}$) over snow-free areas, where
the vegetation is represented as a single-scattering layer above a rough surface, can then be expressed as

$$T_{B\text{toa}.p} = T_{B\text{au}.p} + e^{-\tau_{\text{atm}.p}} T_{B\text{tov}.p} \tag{1}$$

where $T_{B\text{au}.p}$ is the upwelling atmospheric emission and $\tau_{\text{atm}.p}$ is the atmospheric optical depth. Then, respectively, with $T_{B\text{tou}.p}$ the upwelling atmospheric emission [25], $T_{B\text{soil}.p}$ the upward emission of the soil, $T_{B\text{veg}.p}$ the upward and downward emission of the vegetation canopy, $T_{B\text{ad}.p}$ the downward emission of the atmosphere, $r_{r.p}$ the reflectivity of the rough soil surface (equal to $1-e_{r.p}$, with $e_{r.p}$ the emissivity of the soil), and $\tau_{\text{veg}.p}$ the vegetation optical depth. Since the radiometer RPG-6CH-DP is mounted on the ground, $\tau_{\text{atm}.p}$ can be ignored. All optical depths are scaled with the cosine of the viewing angle to account for the corresponding path length extensions. More details about the CMEM model can be found at the website[1] [29], [30], [39]

$$\begin{aligned} T_{B\text{tov}.p} = {} & T_{B\text{soil}.p} e^{-\tau_{\text{veg}.p}} + T_{B\text{veg}.p} \left(1 + r_{r.p} e^{-\tau_{\text{veg}.p}}\right) \\ & + T_{B\text{ad}.p} r_{r.p} e^{-2\tau_{\text{veg}.p}}. \end{aligned} \tag{2}$$

B. Tau-z Model

With a similar optical depth frame, the tau-z model adapts soil optical depth, instead of geometric depth, to define soil moisture sensing depth. The concept of the penetration depth is also described in terms of soil optical depth, i.e., the penetration depth is one time of the soil optical depth in particular. The principal influencing factors determining the penetration depth of microwave bands in soil encompasses the soil's physical and chemical attributes and the frequency and energy of the wavebands. Specifically, physical properties like soil density, moisture content, particle size, and particle size distribution substantially impact microwave penetration depth. Higher soil moisture content and finer soil particles, resulting in increased soil density, typically lead to a shallower penetration depth. Furthermore, chemical properties, such as soil salinity, organic matter content, and mineral composition, also influence the microwave penetration depth. These factors collectively contribute to the soil's dielectric constant, which is a crucial parameter governing microwave propagation and penetration in soil media.

The tau-z model was proposed in 2019 [24] to quantify the relationship between $z_{T\text{eff}}$ and soil optical depth, which is determined by the soil moisture with a fixed wavelength. Wilheit [43] expressed the soil effective temperature (T_{eff}) as follows:

$$T_{\text{eff}} = \int_0^{\infty} T(x)\, \alpha(x) \exp\left[-\int_0^{x} \alpha(x')\, dx'\right] dx \tag{3}$$

where x is the depth from the surface to the soil layer concerned. $T(x)$ is the physical temperature at depth x, and $\alpha(x)$ is an attenuation coefficient determined by dielectric constant ε and wavelength λ. ε' and ε'' are the real/imagery parts of the soil dielectric constant profiles determined primarily by the soil moisture. The detailed form of $\alpha(x)$ is

$$\alpha(x) = \frac{4\pi}{\lambda} \varepsilon''(x) \Big/ 2[\varepsilon'(x)]^{\frac{1}{2}}. \tag{4}$$

With Lv's scheme, soil optical depth τ is traduced in (3) as follows:

$$\tau_x = \int_0^{x} \alpha(x')\, dx'. \tag{5}$$

So, T_{eff} is rewritten as

$$T_{\text{eff}} = \int_0^{+\infty} T(\tau)\, e^{-\tau} d\tau. \tag{6}$$

Compared with (5), (6) takes the integral of soil optical depth τ instead of soil depth x. Subsequently, τ is further replaced with $t = 1-e^{-\tau}$, and (6) evolves to

$$T_{\text{eff}} = \int_0^{1} T(t)\, dt \tag{7}$$

where τ increases with the soil depth. Equation (7) also ignores the coherent characteristics of layered media, as incoherent and coherent frames have affected the result very few [44], [45]. As a τ value corresponds to only one soil depth for a certain soil temperature/moisture combination, we can use τ to replace physical soil depth. Thus, we start with a T profile near the surface, which decays gradually to a constant T profile with depth. Furthermore, since the soil depth is between $[0,+\infty)$ and τ, we can define $t = 1-e^{-\tau} \in [0,1)$

$$\begin{cases} T(\tau) = \int_0^{\tau} (T_{\text{surf}} + a e^{-\tau}\tau) d\tau & (\tau < \tau_{\text{deep}}) \\ T(\tau) = \int_0^{\tau_{\text{deep}}} (T_{\text{surf}} + a e^{-\tau}\tau) d\tau & (\tau \geq \tau_{\text{deep}}) \end{cases} \tag{8}$$

where T_{surf} is the surface temperature, T_{deep} is the soil temperature where it can be considered constant at an annual scale, and τ_{deep} is the soil optical depth corresponding to T_{deep} [24]. Then, to acquire the depth of soil temperature $z_{T\text{eff}}$ (i.e., $\tau_{T\text{eff}}$ in terms of soil optical depth) where the soil temperature equals

[1][Online]. Available: https://confluence.ecmwf.int/display/LDAS/CMEM

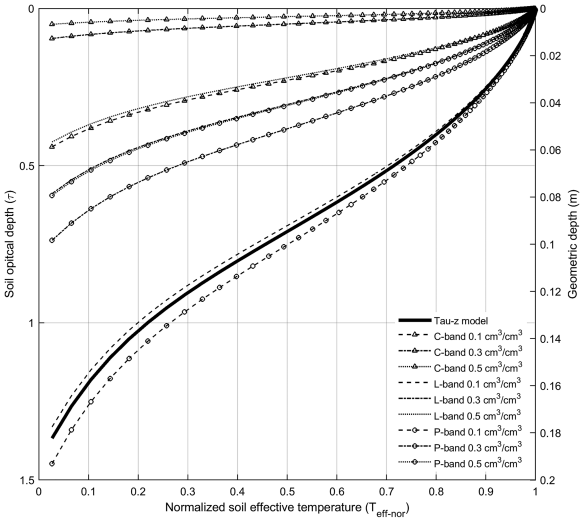

Fig. 4. Soil temperature sensing depth is theoretically inferred from the tau-z model at the *L*-band. Penetration depth is where $\tau = 1$ as a reference.

the soil effective temperature T_{eff} according to the definition of the tau-z model, we solve

$$\tau_{T\text{eff}} = -\ln\left(1 - t\big|_{\frac{T_{\text{eff}}}{T_{\text{deep}} - T_{\text{surf}}} = 1-(1-t)^b\cdot(-\log(1-t)+1)}\right) \tag{9}$$

where $\frac{T_{\text{eff}}}{T_{\text{deep}} - T_{\text{surf}}}$ can be rewritten as $T_{\text{eff}\_\text{nor}}$ [24].

Fig. 4 indicates the relationship between $\tau_{T\text{eff}}$ (left axis)/$z_{T\text{eff}}$ (right axis) and $T_{\text{eff}\_\text{nor}}$ defined by the tau-z model as in (9). Regarding soil optical depth, the τ_{eff}-$T_{\text{eff}\_\text{nor}}$ relationship is not affected by soil moisture. This means that the blue line in Fig. 4 is a fixed line, regardless of soil moisture profiles, soil texture, or other factors that can impact the dielectric constant.

Assuming that the soil moisture profile is unique along with the depth, i.e., $d\tau/dz = \alpha(z) =$ constant, we get a group of red lines to indicate the $z_{T\text{eff}}$ -$T_{\text{eff}\_\text{nor}}$ relationship. At the *C*-band, the soil temperature sensing depth $z_{T\text{eff}}$ ranges from 0 to 0.06 m when the soil moisture is 0.1 cm^3/cm^3, 0–0.01 m for 0.3 cm^3/cm^3, and 0–0.005 m for 0.5 cm^3/cm^3. It means that $z_{T\text{eff}}$ is increasing nonlinearly with larger soil moisture, as higher soil moisture affects soil thermal conductivity and heat capacity, thus influencing the response depth of soil temperature. At the *L*-band, $z_{T\text{eff}}$ ranges from 0 to 0.18 m/0 to 0.08 m/0 to 0.06 m for soil moisture values of 0.1/0.3/0.5 cm^3/cm^3, while at the *P*-band, $z_{T\text{eff}}$ ranges from 0 to 0.2 m/0 to 0.09 m/0 to 0.08 m relatively. The interval for *P*/*L*-bands is almost three times that of the *C*-band, where the difference in $z_{T\text{eff}}$ between *L*- and *P*-bands is always less than 0.02 cm with the same soil moisture and $T_{\text{eff}\_\text{nor}}$. With the soil moisture profile fixed, $z_{T\text{eff}}$ is dominated by the soil temperature profile that varies with the radiation forcing over the ground surface.

C. Statistic Tools

The data assimilation theory generally assumes no bias between observation and simulations. Thus, it is necessary to remove bias as a preprocessing step. The bias is defined as

$$\text{bias} = \frac{1}{n}\sum_{i=1}^{n}(\text{sim} - \text{obs}) \tag{10}$$

sim is the simulated TB from the CMEM model, and obs is the measurement in the experiment. After removing bias, the root-mean-squared error (RMSE) is defined as follows:

$$\text{RMSE} = \sqrt{\frac{1}{n}\sum_{i=1}^{n}(\text{sim} - \text{obs})^2}. \tag{11}$$

The unbiased root-mean-squared error (unRMSE) is defined as follows:

$$\text{unRMSE} = \sqrt{\frac{1}{n}\sum_{i=1}^{n}[\text{reg}(\text{sim}) - \text{obs}]^2} \tag{12}$$

where reg(sim) is the linear regression function between sim and obs as obs = reg(sim) for the least squares method. unRMSE is also a key parameter in data assimilation, as it stands for how much influence the difference between simulation and observations would have on them in terms of mean and covariance, i.e., probability distributions assumed Gaussian. However, CMEM is not a linear model. For example, soil emission is dominated by soil moisture at *L*-bands.

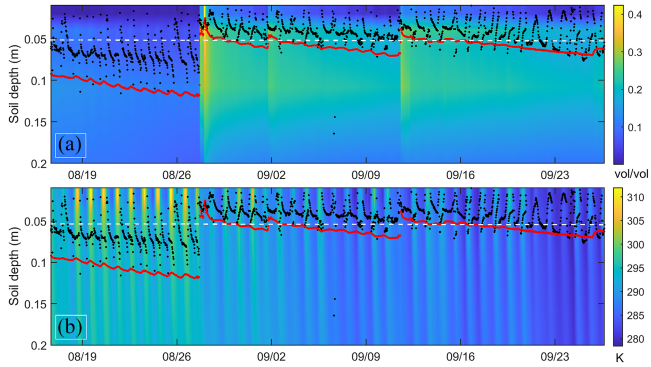

Fig. 5. (a) Soil moisture and (b) soil temperature fields interpolated from observation with 5 cm (white dash) penetration depth (red) and soil temperature sensing depth $z_{T\text{eff}}$ (black dot) during the experiments.

IV. Result

Fig. 5 depicts the experimental results on the penetration depth, variation in v, and the fixed 5-cm interval in the soil temperature and soil moisture profiles. The trends observed in penetration depth and $z_{T\text{eff}}$ are predominantly governed by soil moisture dynamics, specifically the evolution of precipitation and evaporation during the study period. The dryer the soil is, the deeper the penetration depth/$z_{T\text{eff}}$ is. Before the precipitation event on 28 August, the penetration depth was more profound than 0.09 m, with a daily variation of about 0.01 m. In comparison, $z_{T\text{eff}}$ mostly ranged from 0.06 to 0.08 m, with a daily variation of 0.08 m. After the precipitation event on 28 August, the penetration depth and $z_{T\text{eff}}$ vary along the 5 cm, where the amplitude of $z_{T\text{eff}}$ can be 0.09 m daily, depending on the soil temperature changes. In contrast, the daily amplitude of penetration depth is much smaller than that of $z_{T\text{eff}}$ but it

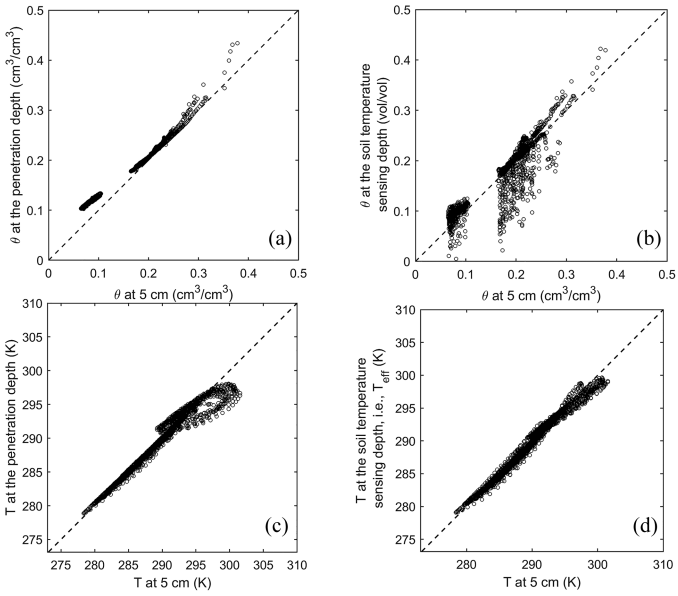

Fig. 6. Soil moisture at (a) 5 cm versus the penetration depth, (b) 5 cm versus $z_{T\text{eff}}$ and soil temperature, (c) 5 cm versus the penetration depth, and (d) 5 cm versus $z_{T\text{eff}}$.

correlates well with precipitation events. In Fig. 5, $z_{T\text{eff}}$ can vary from 1 to 10 cm daily. Since soil temperature has a daily cycle, especially in zones close to the surface, the T_{eff} and the tau-z models derived from the T_{eff} also have solid diurnal cycles. For T_{eff}, the daily cycles refer to the weighting function; for the tau-z model, it is $z_{T\text{eff}}$ dynamics. Using the $z_{T\text{eff}}$, the simulation in this study does not need T_{eff} anymore, so the daily cycle in Fig. 5 compensates for the daily emission changes due to T_{eff}.

Usually, θ at 5 cm is used to validate/calibrate the soil moisture retrievals from *L*-band [23], [46], [47], while the T profiles in the field observation would provide the T_{eff}. Since the impact of T_{eff} is smaller than soil moisture, especially when considering the gradient of θ in the top few centimeters, we compare the soil moisture at the penetration depth and $z_{T\text{eff}}$ with the one gotten from fixed 5 cm in Fig. 6. The result shows that θ at the penetration depth concise with θ at 5 cm very well except at a bias of about 0.02 cm^3/cm^3 when θ<0. 2 cm^3/cm^3 [see Fig. 6(a)]. However, θ at $z_{T\text{eff}}$ is very different to θ at 5 cm. For instance, the θ at $z_{T\text{eff}}$ is generally 0.02–0.04 cm^3/cm^3 higher than θ at 5 cm from 0 to 0.5 cm^3/cm^3 [see Fig. 6(b)]. But 0–0.15 cm^3/cm^3 is lower for some moments from 0.15 to 0.3 cm^3/cm^3 for θ at 5 cm. This implies that the choice of θ input cannot be overlooked in the simulation process of forwarding, as well as in retrieving data or results. Regarding soil temperature, the situation is reversed to the soil moisture, which means T at $z_{T\text{eff}}$ coincides with T at 5 cm better with only a difference of less than 2 K [see Fig. 6(d)]. In contrast, the T at the penetration depth can closely match that T at 5 cm when below 290 K but diverges significantly above this threshold, possibly by up to 8 K, showing apparent daily variation around it [see Fig. 6(c)].

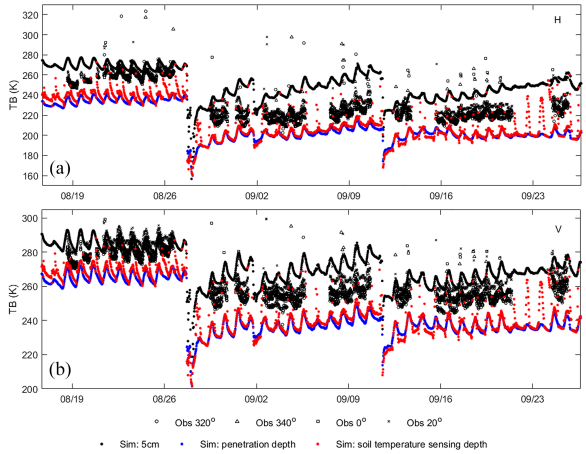

Fig. 7. Time series of TB at the incidence angle of 40° at the *L*-band.

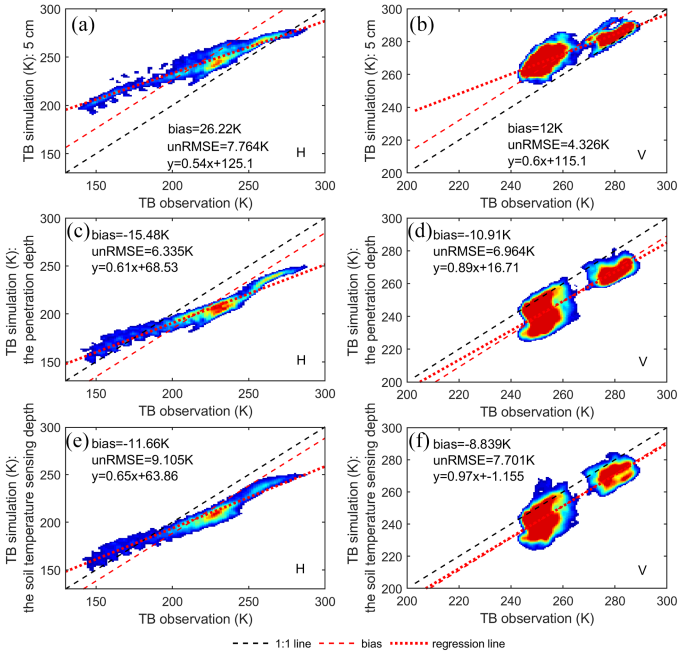

Fig. 8. TB observations mean over at the incidence angle of 40° and the azimuth angles at 320°/340°/0°/20° versus CMEM simulated brightness temperature with soil moisture and temperature at (a) 5 cm in H-polarization, (b) 5 cm in V-polarization, (c) the penetration depth in H-polarization, (d) the penetration depth in V-polarization, (e) the soil temperature sensing depth z_{Teff} in H-polarization and (f) the soil temperature sensing depth z_{Teff} in V-polarization.

The CMEM forwarding TB at the incidence angle of 40° from taking θ and T at 5 cm/the penetration depth/$z_{T\text{eff}}$ is shown in Figs. 7 and 8. Even with the same incidence angle, the difference among azimuth angles at 320°/340°/0°/20° can reach 5 K (see Fig. 7). Compared with the TB observations, the simulation with θ and T at 5 cm is always higher at about 26.22 K/12 K for H/V-polarization. The simulation results with θ and T from the penetration depth and $z_{T\text{eff}}$ are pretty close to each other except for a more substantial daily variation for the latter one. However, both the simulation results with θ and T from the

penetration depth and $z_{T\text{eff}}$ show a negative bias compared with the observations, especially the former. The negative bias is −15.48 K/−10.91 K for H/V-polarization between 5 cm and the penetration depth and −11.66 K/−8.839 K for H/V-polarization between 5 cm and $z_{T\text{eff}}$. The TBs in Fig. 7 are consistent with the dynamics of $z_{T\text{eff}}$ and penetration depth in Fig. 5, where both are more profound than 5 cm most of the time in a day, i.e., higher TBs with lower soil moisture than 5 cm. Only during noon do TBs simulated by the soil temperature sensing depth inputs have a TB result higher than 5 cm because $z_{T\text{eff}}$ is shallower than 5 cm.

Fig. 8 demonstrates that the H-polarization exhibits a more linear relationship between simulations and observations than the V-polarization. Consequently, the H-polarization brightness temperature (TB) is deemed more suitable for data assimilation, as the observation operator can be formulated with greater precision than that of the V-polarization TB. Regarding data assimilation, unRMSE is a more valuable reference than bias regarding soil moisture retrieving. Among the simulation results from taking θ and T at 5 cm/the penetration depth/$z_{T\text{eff}}$, $z_{T\text{eff}}$'s result shows larger unRMSE with values of 9.105 K/7.701 K for H/V than 5 cm, which is 7.764 K/4.326 K, and the penetration depth's, which is 6.335/6.694 K relatively. However, despite its practical significance, unbiased estimation possesses inherent limitations in certain scenarios, potentially rendering it suboptimal compared with other estimators. One significant shortcoming of unbiased estimation lies in its sole reliance on the first moment (mean) as a measure of accuracy. While this simplifies calculations, it poses challenges when faced with multiple unbiased estimates of a parameter, as it becomes difficult to ascertain the most accurate estimator in a specific context. Moreover, in some instances, the variance of the unbiased estimate may be substantial, indicating a greater degree of volatility and instability in the estimation results. Therefore, when evaluating the accuracy of TB simulations, it is crucial to consider unbiasedness and metrics, such as bias and RMSE. The RMSE of $z_{T\text{eff}}$ shows the slightest error, with a value of 12.92 K/11.66 K, much lower than those of 5 cm (30.2 K/20.48 K) and the penetration depth (17.89 K/13.95 K). The biases are also reduced from 26.22 K/12 K for H/V-polarization with fixed 5 cm to −15.48 K/−10.91 K when considering the penetration depth and further to −11.66 K/−8.839 K when considering the soil temperature sensing depth $z_{T\text{eff}}$'s. It should be noted that SMAP requires 0.04 cm^3/cm^3 volumetric soil moisture unRMSE, which is about 16 K in TB for SMELR.

V. Discussion

In the context of passive microwave remote sensing for soil moisture, the soil sensing depth denotes the vertical range of soil layers detectable by remote sensing instrumentation. This depth range is paramount in interpreting and utilizing remote sensing data. First, the soil sensing depth determines how remote sensing data can capture soil moisture variations. Given that soil moisture may vary significantly across different soil depths and that passive microwave remote sensing equipment exhibits varying detection capabilities, a precise knowledge of the soil sensing depth is essential for comprehending the soil moisture status portrayed by remote sensing data. Second, the soil sensing depth also directly impacts remote sensing data's spatial resolution and accuracy. In monitoring and retrieving soil moisture, satellite remote sensing data must be compared and validated against ground-based measurements. If the soil sensing depth of the satellite data does not align with the soil depth of ground measurements, the accuracy and reliability of such comparisons and validations will be compromised. Therefore, a thorough understanding of soil sensing depth in passive microwave remote sensing of soil moisture is pivotal for optimizing the application of this technology in soil moisture monitoring and retrieval, thereby enhancing the accuracy and reliability of remote sensing data interpretation and utilization.

In the passive microwave remote sensing of soil moisture, accurately determining the soil sensing depth is challenging due to the intricate influence of factors, such as soil type, moisture content, and temperature on the soil's dielectric and microwave radiation properties [37]. The dielectric constant of soil serves as a pivotal parameter in determining the dynamic interplay between microwaves and the soil medium, thereby significantly influencing the depth of penetration and detection within the soil. Distinct soil types exhibit varied dielectric constants, resulting in differential effects on microwaves' penetrability and sensing capabilities. Consequently, the specific dielectric constant of the soil type in question must be considered when assessing and determining the optimal soil detection depth. Additionally, soil moisture represents a crucial factor that significantly impacts the soil detection depth. As the moisture content of the soil increases, it leads to alterations in the dielectric constant, thereby modulating the penetration efficacy and sensing depth of microwaves. Therefore, the influence of soil moisture must be duly incorporated into the analysis when estimating and determining the soil detection depth. Furthermore, soil temperature also significantly influences on microwaves' penetration capacity and detection depth. As the soil temperature increases, the penetration ability of microwaves will increase, but at the same time, the impact of soil moisture will also decrease. Therefore, soil temperature's influence must be considered when determining soil detection depth. In summary, choosing soil detection depth is complex in passive microwave remote sensing of soil moisture, and the influence of multiple factors must be comprehensively considered. To accurately determine the soil detection depth, conducting in-depth research on microwave radiation characteristics and dielectric constant changes under different soil types, moisture contents, and temperatures is necessary, as well as establishing the accurate models and algorithms to invert soil moisture.

Fig. 9 and Table III show the CMEM simulations with all incidence angles varying from 30° to 65° (2.5° interval). The azimuth angle varies at 340°, 340°, 0°, and 20° with the depths' definitions of 5 cm, the penetration depth, and soil temperature sensing depth at *L/C/X*-bands with observations collected in the experiment. It can be seen that *C*- and *X*-band observations also have great ranges from 150 to 280 K, but the CMEM has weaker simulation results with a TB interval from 220 to 280 K. The observed values of the *L*-band vary in the range of 150–290 K, and the simulation results corresponding to CMEM are more robust than those of the *C/X*-band and show a certain linear trend in the TB range of 150–2700 K, as CMEM was developed first for the *L*-band. All simulations have a positive bias compared with

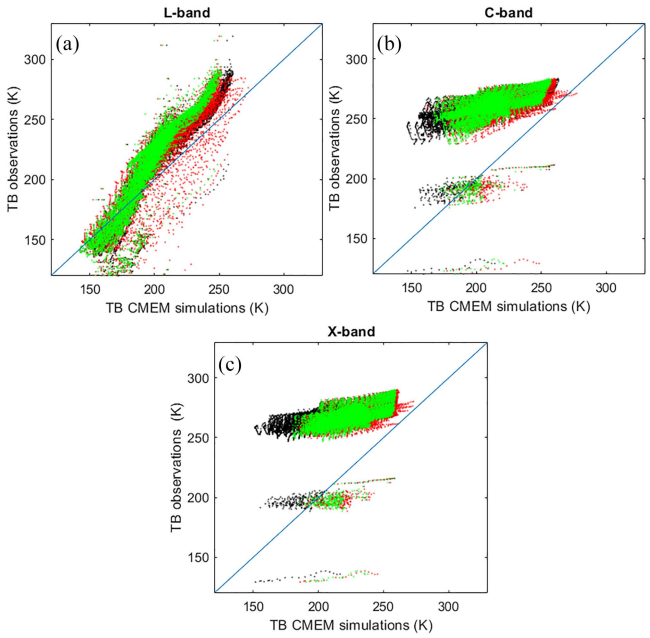

Fig. 9. TB observations from SMELR versus CMEM simulated brightness temperature with soil moisture at (a) *L*-band, (b) *C*-band, and (c) *X*-band with soil moisture and soil temperature inputs from 5 cm (black), the penetration depth (green), and the soil temperature sensing depth (red) with incidence angle varies from 30° to 65° (2.5° interval), and the azimuth angle varies at 340°, 340°, 0°, and 20°.

TABLE III
PARAMETERS IN FIG. 9

Band	Depth inputs	Bias (K)	unRMSE (K)	Regression function
L	5 cm	26.22	10.46	y=1.6x+−167.6
	Penetration depth	15.48	7.87	y=1.5x+−86.11
	soil temperature sensing depth	11.66	9.36	y=1.3x+−55.36
C	5 cm	17.3	3.94	y=0.34x+177.6
	Penetration depth	46.78	4.79	y=0.3x+196.6
	soil temperature sensing depth	40.89	4.90	y=0.28x+198.3
X	5 cm	22.25	4.40	y=0.26x+203.2
	Penetration depth	41.37	4.67	y=0.27x+205.1
	soil temperature sensing depth	37.88	4.7	y=0.26x+208

the observations. However, considering the penetration depth and soil temperature sensing depth, the CMEM simulation results are improved by 5–20 K. For the *C/X*-band, the soil moisture cal/val ground measurements shall be shallower theoretically than the 5 cm assigned in SMAPs cal/val. In fact, 5 cm is also often used for the advanced microwave scanning radiometer 2-the Japan Aerospace Exploration Agency, Fengyun-3 B/C/D, the advanced scatterometer soil moisture retrievals [48], [49], [50], [51], [52], [53], [54], and other merged soil moisture products, such as ECMWF reanalysis fifth-generation land, the modern-era retrospective analysis for research and applications, version 2, and the ESAs climate change initiative for soil moisture [55], [56], [57], [58].

The moisture and temperature sensing depths are not the same but should be consistent. The tau-z model can formulate the soil temperature sensing depth because the surface and deep soil temperatures can be sensed or assumed as constant, and the soil temperature profiles can sometimes fit the monotonic hypothesis at a specific time of the day [36]. However, these assumptions, hypotheses, and data sources don't exist regarding soil moisture profile. Thus, it is still unsettled to formulate the soil moisture sensing depth in math. In this case, the depth of moisture and temperature sensing are not the same, but their increase/decrease shall be consistent, as T_{eff} was created to compensate for the impact of soil moisture on soil temperature weightings [59]. If the soil surface is wet, the soil optical depth changes, so soil moisture and temperature sensing depths are closer to the surface. Otherwise, both will be closer to the soil moisture/temperature in a deeper layer.

Additionally, the study of *L*-band passive microwave sensing depth using the tau-z model has many significant points. First, the tau-z model helps better understand the effects of soil moisture and other relevant parameters on microwave penetration depth. Second, the tau-z model facilitates a deeper understanding of the interaction mechanism between microwaves and soil. It further helps improve the accuracy and reliability of microwave remote sensing technology and provides valuable references for other related fields (such as radar remote sensing and groundwater detection). In addition, the tau-z model will also contribute to the development and application of related technologies. For example, by improving microwave detection technology, its sensitivity and accuracy to soil moisture can be improved, thereby providing better technical support for emerging fields, such as precision agriculture and smart agriculture. Finally, the tau-z model also helps promote interdisciplinary collaboration and communication. Since microwave detection involves multiple disciplines (such as physics, soil science, and agriculture), research on sensing depth can foster cross integration and drive innovation in related fields.

The upcoming satellite mission of the Copernicus microwave imaging radiometer and the Chinese ocean salinity satellite will carry a radiometer spanning the *L*-band to the Ka-band. While this unique design will help enhance the retrieval accuracy of soil moisture, attention should be paid when using multifrequency observations [31]. It is commonly assumed that the penetration/sensing depth is equal across different frequencies [49]. It is expected to provide the sensing depth in global soil moisture products. The tau-z model, which describes the effective sensing depth of microwaves, can play a significant role in microwave remote sensing of soil moisture and temperature profiles. This can be achieved using a low-frequency, wideband radiometer [60], or a multifrequency and multiangular radiometer [35].

VI. CONCLUSION

This work takes the soil moisture, soil temperature, and other inputs from the comprehensive remote sensing experiment of the

water cycle and energy balance in SMELR for the TB simulation with CMEM. It compares the result with the TB observation at various incidence and azimuth angles. Since we take the CMEM with Fresnel's mode, the soil moisture and soil temperature are prepared according to three different depth definitions: fixed 5 cm, the penetration depth, and the soil temperature sensing depth offered by the tau-z model. The result shows the following.

1) The bias can be reduced from 26.22 K/12 K for H/V-polarization with fixed 5 cm to −15.48 K/−10.91 K by considering the penetration depth and to −11.66 K /−8.839 K by considering the soil temperature sensing depth.
2) RMSE can be reduced from 30.2 K/20.48 K for H/V-polarization with fixed 5 cm to 17.89 K/13.95 K by considering the penetration depth and to 12.92 K/11.66 K by considering the soil temperature sensing depth.
3) For unRMSE, the soil temperature sensing depth is superior to the other two depths.

We hope that this study can provide valuable information for studying multiband passive microwave detection depth to understand soil properties, improve remote sensing technology, and promote interdisciplinary cooperation.

ACKNOWLEDGMENT

The authors sincerely appreciate all the contributors to the dataset used in this study.

REFERENCES

[1] S. Hagemann and T. Stacke, "Impact of the soil hydrology scheme on simulated soil moisture memory," *Climate Dyn.*, vol. 44, pp. 1731–1750, 2015.
[2] T. Yasunari, "Role of land-atmosphere interaction on Asian monsoon climate," *J. Meteorol. Soc. Jpn.*, vol. 85B, pp. 55–75, Jul. 2007.
[3] C. Klein and C. M. Taylor, "Dry soils can intensify mesoscale convective systems," *PNAS*, vol. 117, no. 35, pp. 21132–21137, 2020.
[4] W. Liu, Q. Zhang, C. Li, L. Xu, and W. Xiao, "The influence of soil moisture on convective activity: A review," *Theor. Appl. Climatol.*, vol. 149, no. 1, pp. 221–232, 2022.
[5] B. van den Hurk, M. Best, P. Dirmeyer, A. Pitman, J. Polcher, and J. Santanello, "Acceleration of land surface model development over a decade of glass," *Bull. Amer. Meteorol. Soc.*, vol. 92, no. 12, pp. 1593–1600, Dec. 2011.
[6] A. Boone et al., "The AMMA land surface model intercomparison project (ALMIP)," *Bull. Amer. Meteorol. Soc.*, vol. 90, no. 12, pp. 1865–1880, 2009.
[7] L. Deqin, Z. Shuwen, W. Xiaohang, and H. Hui, "Soil moisture parameterization and its influences in weather and climate simulation: A review," *Adv. Earth Sci.*, vol. 31, no. 3, 2016, Art. no. 236.
[8] M. Stefanon, P. Drobinski, F. D'Andrea, C. Lebeaupin-Brossier, and S. Bastin, "Soil moisture-temperature feedbacks at meso-scale during summer heat waves over Western Europe," *Climate Dyn.*, vol. 42, no. 5/6, pp. 1309–1324, Mar. 2014.
[9] T. J. Jackson, A. Y. Hsu, A. Van de Griend, and J. R. Eagleman, "Skylab L-band microwave radiometer observations of soil moisture revisited," *Int. J. Remote Sens.*, vol. 25, no. 13, pp. 2585–2606, Jul. 2004.
[10] W. D. Compton and C. D. Benson, *Living and Working in Space: A History of Skylab*. Washington, DC, USA: Scientific and Technical Information Branch, National Aeronautics and Space Administration, 1983.
[11] M. Drusch, T. Holmes, P. de Rosnay, and G. Balsamo, "Comparing ERA-40-based L-band brightness temperatures with skylab observations: A calibration/validation study using the community microwave emission model," *J. Hydrometeorol.*, vol. 10, no. 1, pp. 213–226, Feb. 2009.
[12] J. R. Eagleman and W. C. Lin, "Remote sensing of soil moisture by a 21-cm passive radiometer," *J. Geophys. Res.*, vol. 81, no. 21, pp. 3660–3666, 1976.
[13] S. Paloscia, G. Macelloni, E. Santi, and T. Koike, "A multifrequency algorithm for the retrieval of soil moisture on a large scale using microwave data from SMMR and SSM/I satellites," *IEEE Trans. Geosci. Remote Sens.*, vol. 39, no. 8, pp. 1655–1661, Aug. 2001.
[14] E. G. Njoku, T. J. Jackson, V. Lakshmi, T. K. Chan, and S. V. Nghiem, "Soil moisture retrieval from AMSR-E," *IEEE Trans. Geosci. Remote Sens.*, vol. 41, no. 2, pp. 215–229, Feb. 2003.
[15] Y. Zhang, W. Han, H. Zhang, X. Niu, and G. Shao, "Evaluating soil moisture content under maize coverage using UAV multimodal data by machine learning algorithms," *J. Hydrol.*, vol. 617, Feb. 2023, Art. no. 129086.
[16] Y. H. Kerr, P. Waldteufel, J.-P. Wigneron, J. Martinuzzi, J. Font, and M. Berger, "Soil moisture retrieval from space: The soil moisture and ocean salinity (SMOS) mission," *IEEE Trans. Geosci. Remote Sens.*, vol. 39, no. 8, pp. 1729–1735, Aug. 2001.
[17] Y. Bai et al., "A multi-temporal and multi-angular approach for systematically retrieving soil moisture and vegetation optical depth from SMOS data," *Remote Sens. Environ.*, vol. 280, Oct. 2022, Art. no. 113190.
[18] D. Entekhabi et al., "The soil moisture active passive (SMAP) mission," *Proc. IEEE*, vol. 98, no. 5, pp. 704–716, May 2010.
[19] Z. Peng et al., "First mapping of polarization-dependent vegetation optical depth and soil moisture from SMAP L-band radiometry," *Remote Sens. Environ.*, vol. 302, Mar. 2024, Art. no. 113970.
[20] O. Skulovich and P. Gentine, "A long-term consistent artificial intelligence and remote sensing-based soil moisture dataset," *Sci. Data*, vol. 10, no. 1, Mar. 2023, Art. no. 154.
[21] X. Li et al., "A new SMAP soil moisture and vegetation optical depth product (SMAP-IB): Algorithm, assessment and inter-comparison," *Remote Sens. Environ.*, vol. 271, Mar. 2022, Art. no. 112921.
[22] S. Zhou et al., "Soil moisture–atmosphere feedbacks mitigate declining water availability in drylands," *Nature Climate Change*, vol. 11, no. 1, pp. 38–44, Jan. 2021.
[23] S. Lv, Y. Zeng, J. Wen, D. Zheng, and Z. Su, "Determination of the optimal mounting depth for calculating effective soil temperature at L-band: Maqu case," *Remote Sens.*, vol. 8, no. 6, 2016, Art. no. 476.
[24] S. Lv, Y. Zeng, Z. Su, and J. Wen, "A closed-form expression of soil temperature sensing depth at L-band," *IEEE Trans. Geosci. Remote Sens.*, vol. 57, no. 7, pp. 4889–4897, Jul. 2019.
[25] F. T. Ulaby, R. K. Moore, and A. K. Fung, *Microwave Remote Sensing: Active and Passive: From Theory to Applications*, vol. 3. Norwood, MA, USA: Artech House, 1986.
[26] F. T. Ulaby, M. C. Dobson, and D. R. Brunfeldt, "Improvement of moisture estimation accuracy of vegetation-covered soil by combined active/passive microwave remote sensing," *IEEE Trans. Geosci. Remote Sens.*, vol. GE-21, no. 3, pp. 300–307, Jul. 1983.
[27] F. T. Ulaby, M. Razani, and M. C. Dobson, "Effects of vegetation cover on the microwave radiometric sensitivity to soil moisture," *IEEE Trans. Geosci. Remote Sens.*, vol. GE-21, no. 1, pp. 51–61, Jan. 1983.
[28] S. Lv, C. Simmer, Y. Zeng, J. Wen, and Z. Su, "The simulation of L-band microwave emission of frozen soil during the thawing period with the community microwave emission model (CMEM)," *J. Remote Sens.*, vol. 2022, Oct. 2022, Art. no. 9754341.
[29] Y. Hirahara, P. D. Rosnay, and G. Arduini, "Evaluation of a microwave emissivity module for snow covered area with CMEM in the ECMWF integrated forecasting system," *Remote Sens.*, vol. 12, no. 18, 2020, Art. no. 2946.
[30] M. Lange and P. de Rosnay, "Evaluation of a microwave emissivity module for desert regions with CMEM," *Earth Space Sci.*, vol. 6, no. 9, pp. 1787–1795, 2019.
[31] X. Shen et al., "Soil moisture retrieval depth of P- and L-band radiometry: Predictions and observations," *IEEE Trans. Geosci. Remote Sens.*, vol. 59, no. 8, pp. 6814–6822, Aug. 2021.
[32] S. Lv, B. Schalge, P. S. Garfias, and C. Simmer, "Required sampling density of ground-based soil moisture and brightness temperature observations for calibration and validation of L-band satellite observations based on a virtual reality," *Hydrol. Earth Syst. Sci.*, vol. 24, no. 4, pp. 1957–1973, 2020.
[33] N. Boopathi et al., "Towards soil moisture retrieval using tower-based P-band radiometer observations," in *Proc. IEEE Int. Geosci. Remote Sens. Symp.*, 2018, pp. 1407–1410.
[34] S. Yueh, R. Shah, X. Xu, K. Elder, and B. Starr, "Experimental demonstration of soil moisture remote sensing using P-band satellite signals of opportunity," *IEEE Geosci. Remote Sens. Lett.*, vol. 17, no. 2, pp. 207–211, Feb. 2020.
[35] T. Zhao et al., "Retrievals of soil moisture and vegetation optical depth using a multi-channel collaborative algorithm," *Remote Sens. Environ.*, vol. 257, 2021, Art. no. 112321.

[36] R. H. Reichle et al., "Version 4 of the SMAP level-4 soil moisture algorithm and data product," *J. Adv. Model. Earth Syst.*, vol. 11, no. 10, pp. 3106–3130, Oct. 2019.
[37] B. Usowicz, M. Lukowski, and J. Lipiec, "The SMOS-derived soil water extent and equivalent layer thickness facilitate determination of soil water resources," *Sci. Rep.*, vol. 10, no. 1, Oct. 2020, Art. no. 18330.
[38] T. Zhao et al., "Soil moisture experiment in the Luan River supporting new satellite mission opportunities," *Remote Sens. Environ.*, vol. 240, Apr. 2020, Art. no. 111680.
[39] P. de Rosnay et al., "Soil moisture remote sensing for numerical weather prediction: L-band and C-band emission modeling over land surfaces, the community microwave emission model (CMEM)," in *Proc. IEEE Int. Geosci. Remote Sens. Symp.*, vol. 2, 2008, pp. II–563–II–566.
[40] P. D. Rosnay, M. Drusch, and J. I. M. N. Sabater, "Milestone 1 tech note—Part 1: SMOS global surface emission model," in *Progress Report for ESA Contract*, Shinfield Park, Reading, 2009:ESA Contract 3-11640/06/I-LG, 2009.
[41] S. Lv, Y. Zeng, J. Wen, and Z. Su, "A reappraisal of global soil effective temperature schemes," *Remote Sens. Environ.*, vol. 183, pp. 144–153, Sep. 2016.
[42] S. Lv, J. Wen, Y. Zeng, H. Tian, and Z. Su, "An improved two-layer algorithm for estimating effective soil temperature in microwave radiometry using in situ temperature and soil moisture measurements," *Remote Sens. Environ.*, vol. 152, pp. 356–363, 2014.
[43] T. T. Wilheit, "Radiative transfer in a plane stratified dielectric," *IEEE Trans. Geosci. Electron.*, vol. 16, no. 2, pp. 138–143, Apr. 1978.
[44] F. Brakhasi et al., "Towards soil moisture profile estimation in the root zone using L- and P-band radiometer observations: A coherent modelling approach," *Sci. Remote Sens.*, vol. 7, Jun. 2023, Art. no. 100079.
[45] F. Brakhasi et al., "Soil moisture profile estimation under bare and vegetated soils using combined L-band and P-band radiometer observations: An incoherent modeling approach," *Remote Sens. Environ.*, vol. 307, Jun. 2024, Art. no. 114148.
[46] S. Lv, Y. Zeng, J. Wen, H. Zhao, and Z. Su, "Estimation of penetration depth from soil effective temperature in microwave radiometry," *Remote Sens.*, vol. 10, no. 4, 2018, Art. no. 519.
[47] A. Colliander et al., "Validation of SMAP surface soil moisture products with core validation sites," *Remote Sens. Environ.*, vol. 191, pp. 215–231, Mar. 2017.
[48] C. S. Kang et al., "Global soil moisture retrievals from the Chinese FY-3D microwave radiation imager," *IEEE Trans. Geosci. Remote Sens.*, vol. 59, no. 5, pp. 4018–4032, May 2021.
[49] L. Hu et al., "A twenty-year dataset of soil moisture and vegetation optical depth from AMSR-E/2 measurements using the multi-channel collaborative algorithm," *Remote Sens. Environ.*, vol. 292, Jul. 2023, Art. no. 113595.
[50] J. Y. Du et al., "Inter-calibration of satellite passive microwave land observations from AMSR-E and AMSR2 using overlapping FY3B-MWRI sensor measurements," *Remote Sens.*, vol. 6, no. 9, pp. 8594–8616, Sep. 2014.
[51] S. Kim, Y. Y. Liu, F. M. Johnson, R. M. Parinussa, and A. Sharma, "A global comparison of alternate AMSR2 soil moisture products: Why do they differ?," *Remote Sens. Environ.*, vol. 161, pp. 43–62, May 2015.
[52] Y. Chen et al., "Evaluation of SMAP, SMOS, and AMSR2 soil moisture retrievals against observations from two networks on the Tibetan Plateau," *J. Geophys. Res., Atmos.*, vol. 122, no. 11, 2017, Art. no. 2016JD026388.
[53] X. Zhang, T. Zhang, P. Zhou, Y. Shao, and S. Gao, "Validation analysis of SMAP and AMSR2 soil moisture products over the United States using ground-based measurements," *Remote Sens.*, vol. 9, no. 2, Feb. 2017, Art. no. 104.
[54] J. Du et al., "Assessing global surface water inundation dynamics using combined satellite information from SMAP, AMSR2 and Landsat," *Remote Sens. Environ.*, vol. 213, pp. 1–17, Aug. 2018.
[55] A. Gruber, T. Scanlon, R. van der Schalie, W. Wagner, and W. Dorigo, "Evolution of the ESA CCI soil moisture climate data records and their underlying merging methodology," *Earth Syst. Sci. Data*, vol. 11, no. 2, pp. 717–739, May 2019.
[56] R. H. Reichle et al., "Assessment of MERRA-2 land surface hydrology estimates," *J. Climate*, vol. 30, no. 8, pp. 2937–2960, Apr. 2017.
[57] Z. Wu, H. Feng, H. He, J. Zhou, and Y. Zhang, "Evaluation of soil moisture climatology and anomaly components derived from ERA5-land and GLDAS-2.1 in China," *Water Resour. Manage.*, vol. 35, no. 2, pp. 629–643, Jan. 2021.
[58] P. Lal, G. Singh, N. N. Das, A. Colliander, and D. Entekhabi, "Assessment of ERA5-land volumetric soil water layer product using in situ and SMAP soil moisture observations," *IEEE Geosci. Remote Sens. Lett.*, vol. 19, no. 2508305, pp. 1–5, 2022.
[59] B. J. Choudhury, T. J. Schmugge, and T. Mo, "A parameterization of effective soil temperature for microwave emission," *J. Geophys. Res., Oceans*, vol. 87, no. C2, pp. 1301–1304, 1982.
[60] J. T. Johnson et al., "Microwave radiometry at frequencies from 500 to 1400 MHz: An emerging technology for Earth observations," *IEEE J. Sel. Topics Appl. Earth Observ. Remote Sens.*, vol. 14, pp. 4894–4914, Apr. 2021.

Shaoning Lv received the first Ph.D. degree from Cold and Arid Regions Environmental and Engineering Research Institute, Chinese Academy of Sciences, Lanzhou, China, in 2014, and the second Ph.D. degree from Water Resources Department, Faculty of Geo-Information Science and Earth Observation, University of Twente, Enschede, The Netherlands, in 2019.

He is currently with the Department of Atmospheric and Oceanic Sciences, Institute of Atmospheric Sciences, Fudan University, Shanghai, China. His research interests include passive microwave remote sensing of soil moisture and its application in climate forecast.

Tianjie Zhao (Senior Member, IEEE) received the B.S. and Ph.D. degrees in cartography and geographic information system from Beijing Normal University, Beijing, China, in 2007 and 2012, respectively.

From 2010 to 2012, he was a Visiting Scientist with Hydrology and Remote Sensing Laboratory, Agricultural Research Service (ARS), U.S. Department of Agriculture, Beltsville, MD, USA. He is currently a Research Professor with the State Key Laboratory of Remote Sensing Science, Aerospace Information Research Institute, Chinese Academy of Sciences (CAS), Beijing, China. His research interests include microwave remote sensing of soil moisture and its freeze-thaw process.

Dr. Zhao was a recipient of the Scholarship Award for excellent doctoral student granted by the Ministry of Education of China in 2011, the Young Scientist Award from the International Union of Radio Science (URSI) in 2014, the Young Scientist Award from Progress in Electromagnetics Research Symposium (PIERS) in 2018, and the Li Xiaowen Youth Award in Remote Sensing Science in 2023.

Yin Hu received the B.S. degree in geographic information science from the School of Mining Engineering, North China University of Science and Technology, Tangshan, China, in 2022. She is currently working toward the M.S. degree in atmospheric science with the Department of Atmospheric and Oceanic Sciences (Institute of Atmospheric Sciences), Fudan University, Shanghai, China.

Her research interests include microwave remote sensing of soil freeze-thaw process.

Jun Wen received the B.A. degree in meteorology from Peking University, Beijing, China, in 1988, the M.A. degree in meteorology from Lanzhou University, Lanzhou, China, in 1995, and the Ph.D. degree in meteorology from the Chinese Academy of Sciences, Lanzhou, in 1999.

He is currently a Professor with the College of Atmospheric Sciences, Chengdu University of Information Technology, Chengdu, China. His research interests include remote sensing and data assimilation, land surface modeling, and climate change.